The 2-D Model of the Flow around a Modified Rotary Viscometer

L.D. Hird, P.F. Siew & S. Wang
Curtin University of Technology,
GPO Box U1987, Perth, Western Australia 6845

Abstract

A rotary viscometer, consisting of a rotating rotor surrounded by a slotted sleeve, is placed eccentrically within a rotating bowl. Using both Newtonian fluids (of large Reynolds number) and power law (shear-thinning) fluids, a finite volume method is used to model the two-dimensional flow around the viscometer. Contour plots of the streamlines are shown for various eccentricities, rotational speeds, Reynolds numbers and power law indices and the effect of these parameters on the flow field is discussed.

1 INTRODUCTION

This paper looks at the numerical simulation of the unsteady, isothermal flows of incompressible, viscous, generalised Newtonian fluids, between two eccentric rotating cylinders with a slotted sleeve placed around the inner cylinder. The setup is a two-dimensional model of a viscometer, developed by Overend et al [1984], used to estimate the rheological properties of settling slurries and assumes that end effects in the viscometer are unimportant (see Fig. 1). The bounding cylinders are assumed to rotate uniformly in opposite directions. This paper uses a finite volume method to approximate the flow fields developed by Newtonian and shear-thinning fluids. The flow patterns obtained will aid in assessing the effectiveness of the viscometer used in practice.

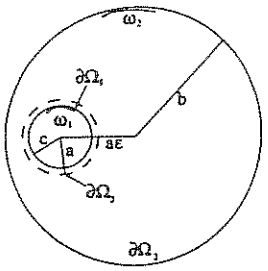

Figure 1: The two-dimensional model.

1.1 Governing Differential Equations and Boundary Conditions

Let Ω represent the region of the xy-plane, between the two cylinders, with origin at the centre of the rotor, and let $\partial\Omega_1$ and $\partial\Omega_2$ denote the rotor and bowl, respectively. Also let $\partial\Omega_3^q (q = 1, \ldots, s)$ denote the surface elements of the sleeve consisting of s surface elements (see Fig. 1). At a point $\boldsymbol{x}$ $(= (x_i, y_i))$ in Ω and at a given time $t \in$ (0,T], the unsteady, isothermal flows of incompressible, viscous, generalised Newtonian fluids in the domain Ω can be modelled using the (dimensionless) stream and vorticity functions, viz

$$\begin{aligned} \frac{\partial \zeta}{\partial t} - \nabla \cdot (Sh\nabla\zeta - [\mathbf{v} + S\nabla h]\,\zeta) &= \\ & 2S\,(\nabla \times [\nabla h \cdot \nabla]\,\mathbf{v}) \cdot \mathbf{k}, \\ \nabla^2\psi + \zeta = 0, \qquad & \text{and} \quad h(\dot\gamma) = k_1 \dot\gamma^{\alpha-1}. \end{aligned} \tag{1.1}$$

$S = \dfrac{\tau_o}{\rho a b \omega_2 \dot\gamma_o}$ is a dimensionless group where τ_o and $\dot\gamma_o$ are representative values of the stress and shear rate. $h(\dot\gamma)$ represents the dimensionless apparent viscosity

function where $\dot{\gamma} = \sqrt{2\,(\dot{\gamma}_{ij} : \dot{\gamma}_{ij})}$. When $\alpha = 1$, the fluid is Newtonian and the first equation in (1.1) reduces to a homogeneous advection-diffusion equation where Sh becomes the reciprocal of the Reynolds number $Re = ab\omega_2/\nu$. No-slip and no-penetration conditions are prescribed on the solid surfaces and the stream function is defined so that $\psi = 0$ on the rotor and $\psi = K_2$ and $\psi = K_3^q$ on the bowl and slotted sleeve, respectively. Equation (1.1) represents a nonlinearly coupled system of equations; however, we will decouple this system where at each time step, the discretised governing equations are solved in sequence. We seek the steady-state solution to the above transient problem.

1.2 Discretisation and Assembly

Integrating the first equation in (1.1) over each tessellation (d_i) and applying Green's theorem yields

$$\int_{d_i} \frac{\partial \zeta}{\partial t} dA - \int_{\partial d_i} \mathbf{F}_1 \cdot \mathrm{n} ds = \int_{\partial d_i} \mathrm{f} \cdot \mathrm{t} ds, \qquad (1.2)$$

where

$$\mathbf{F}_1 = Sh\nabla\zeta - [\mathrm{v} + S\nabla h]\,\zeta, \qquad (1.3)$$

and

$$\mathrm{f} = 2S\,(\nabla h \cdot \nabla)\,\mathrm{v}. \qquad (1.4)$$

Writing $\mathrm{f} \cdot \mathrm{t} = \mathbf{F}_2 \cdot \mathrm{n}$ and assuming ζ is piecewise constant over each tessellation, equation (1.2) can be written as

$$\frac{\partial \zeta_i}{\partial t}|d_i| - \sum_{j \in I_i} \int_{l_{ij}} (\mathbf{F}_1 + \mathbf{F}_2) \cdot \mathrm{n} ds = 0, \qquad i = 1, 2, \ldots, N_\nu \qquad (1.5)$$

where $\mathbf{F}_2 = (\mathrm{f} \times \mathrm{k})$, $\zeta_i = \zeta(\boldsymbol{x}_i, t)$, $|d_i|$ denotes the area of d_i and I_i represents the index set of neighbouring nodes to the interior node $\boldsymbol{x}_i$. Also, N_ν denotes the number of interior nodes. The notation used here to denote the edges and nodes of the dual meshes is understood from Fig. 2. As the integrations in (1.5) are performed along the sides of a control volume, we introduce a coordinate system, local to each side l_{ij}, defined by the unit outward and tangential vectors n and t respectively (see Fig. 2). Thus, along each l_{ij},

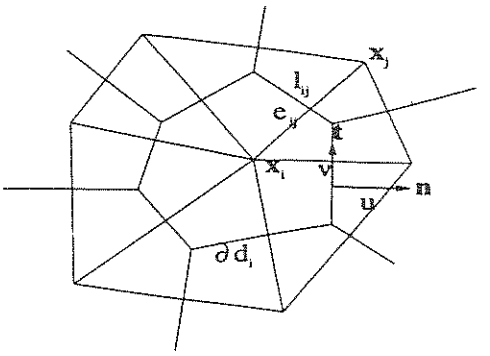

Figure 2: The Voronoi tessellation and Delaunay triangulation around a mesh node.

$\mathbf{F}_1$, $\mathbf{F}_2$ and $h(\dot{\gamma})$ are given by

$$\mathbf{F}_1 = \left[Sh\frac{\partial \zeta}{\partial n} - \left(u + S\frac{\partial h}{\partial n}\right)\zeta, Sh\frac{\partial \zeta}{\partial t} - \left(v + S\frac{\partial h}{\partial t}\right)\zeta, 0\right] \qquad (1.6)$$

$$\mathbf{F}_2 = (\mathrm{f} \times \mathrm{k}) = 2S\left[\frac{\partial h}{\partial n}\frac{\partial v}{\partial n} + \frac{\partial h}{\partial t}\frac{\partial v}{\partial t}, -\frac{\partial h}{\partial n}\frac{\partial u}{\partial n} - \frac{\partial h}{\partial t}\frac{\partial u}{\partial n}, 0\right] \qquad (1.7)$$

and

$$h(\dot{\gamma}) = k_1\left[\zeta^2 - 4\frac{\partial(u,v)}{\partial(n,t)}\right]^{\frac{\alpha-1}{2}}, \qquad (1.8)$$

where u and v denote the velocity in the directions of n and t respectively.

Equation (1.5) can be simplified if u is assumed constant along each l_{ij}. Further, following the finite volume method used by Miller and Wang [1994], (1.5) is approximated by

$$\frac{\partial \zeta_i}{\partial t}|d_i| - \sum_{j \in I_i} \frac{Sh_i|l_{ij}|}{|e_{ij}|}\left[B(m_{ij})\,\zeta_j - B(-m_{ij})\,\zeta_i\right] = 0 \qquad (1.9)$$

where $m_{ij} = \dfrac{\bar{u}_{ij} - S\bar{h}_{ij}}{Sh_i}|e_{ij}|$ and $\bar{u}_{ij}$ and $\bar{h}_{ij}$ approximate u and $\partial h/\partial \mathrm{n}$ along n. $B(x)$ represents the Bernoulli function and along l_{ij}, $h(\dot{\gamma}) \approx k_1|\zeta|^{\alpha-1}$. We now introduce the implicit time discretisation

$$\frac{\partial \zeta_i}{\partial t} = \frac{\zeta_i^k - \zeta_i^{k-1}}{\Delta t_k} \quad \text{and} \quad \zeta_i = c\zeta_i^k + (1-c)\zeta_i^{k-1}. \qquad (1.10)$$

The backward-Euler and Crank-Nicholson schemes correspond to $c = 1$ and $c = 1/2$ respectively. Therefore, for a given time sub-interval $[t_{k-1}, t_k] \in$ (0,T], the system of linear equations generated from (1.9) to deter-

mine the vorticity at each time step is given by

$$\left(I + cD^k\right) Z^k - E^k = \left(I + [c-1]D^k\right) Z^{k-1}, \quad (1.11)$$

where E^k depends on the boundary conditions, for vorticity, at the no-slip surfaces. These boundary conditions can be estimated using the Poisson equation and Dirichlet conditions for the stream function.

The Poisson equation in (1.1) can be discretised to determine the stream function field at each time step, whence

$$A\Psi^k + B^k = Z^k. \quad (1.12)$$

At each time step, $\dot{\gamma}$ is estimated from

$$\dot{\gamma}_i^k = \left|\zeta_i^k\right|, \qquad i = 1, 2, \ldots. \quad (1.13)$$

Using the bi-viscosity model of Tanner and Milthorpe [1983], a well-behaved viscosity function over each tessellation can be determined, viz

$$h_i^k = \begin{cases} k_1 \left(\dot{\gamma}_i^k\right)^{\alpha-1} & \text{for} \quad \dot{\gamma}_i^k > \dot{\gamma}_c, \\ k_1 \left(\dot{\gamma}_c\right)^{\alpha-1} & \text{for} \quad \dot{\gamma}_i^k \leq \dot{\gamma}_c. \end{cases} \quad (1.14)$$

As K_2 and K_3^q are not known a priori, at each time step they are estimated from the neighbouring nodes to the no-slip surfaces. Equations (1.11), (1.12) and (1.14) represent a non-linearly coupled system; however, this system can be linearised by solving the three equations in sequence.

1.3 Solution Process

The non-linear system given by equations (1.11), (1.12) and (1.14) is decoupled into a system of three linear equations. An iterative scheme is used to accomplish this where the outer (non-linear) iteration is performed only once per time step. At the inner level, each of the linear equations (i.e., equations (1.11) and (1.12)) is solved using the CGS method given by Sonneveld [1989]. Incomplete LU factorisation is used to precondition the matrices. Due to the lack of information for the Dirichlet boundary conditions for the stream function, the discretised Poisson equation and estimates $\bar{K}_2$ and $\bar{K}_3^q$ are solved repeatedly until self-consistent solutions are obtained. The numerical stability of the solver for equations (1.11) and (1.12) is ensured since, for all problems considered, the coefficient matrices $I + cD^k$ and A can be shown to be M-matices. At the end of each time step (i.e., each outer iteration), the scalar fields for the stream, vorticity and viscosity functions are stored. Convergence is established when the difference in each of the three scalar fields, over a prescribed time period, is small. The convergence criteria becomes increasingly more difficult to satisfy as either S or $|\bar{U}|$ (the magnitude of the relative rotational speed of the rotor) become large or when α is made small. The rate of convergence of the iterative scheme is at best linear and is affected by the initial guess and also by the length of the time step, Δt_k, used. The choice of initial guess depends on the parameters $\{S, \alpha, \bar{U}\}$ to be solved. If the flow pattern is wanted for large S or $|\bar{U}|$, we use the steady-state (i.e., converged) solution to a problem with smaller S or $|\bar{U}|$ as the initial guess. A similar process is used when obtaining steady-state solutions for small α, i.e., the steady-state solution for higher α is used as the inital guess. We also note that some smoothing of the vorticity and viscosity is done at each time step; this enhances the stability of the interative scheme. As small time steps are used in our solution process, we discretise the time component using the Crank-Nicholson scheme; thus, we put $c = 1/2$ in equation (1.11).

2 RESULTS

For the contour plots presented here, a spacing of 0.2 between each streamline is used. We first consider the case when the flow domain is filled with a Newtonian fluid and then discuss the developed flow when pseudoplastic (shear-thinning) fluids are used.

2.1 Newtonian Fluids

In this section, we consider moderate- to high- Reynolds number flow only. For an analytic treatment in the low Reynolds number limit, the interested reader is referred to Hird and Siew [1996]. Consider the problems $\{500.0, 0.2, -5.0\}$, $\{500.0, 0.5, -5.0\}$ and $\{500.0, 0.7, -5.0\}$ where the first term represents the Reynolds number (Re), the second term represents the eccentricity ratio ($\bar{\epsilon} = a\epsilon/(b-a)$) and the third term represents $\bar{U}$ ($= c\omega_1/b\omega_2$). The solution fields are given in Fig. 3.

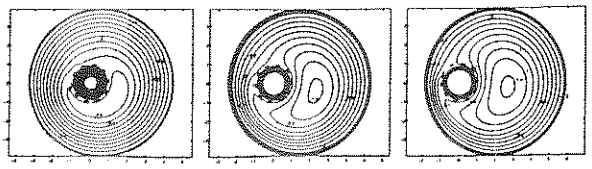

Figure 3: Contour plots in the entire flow field and around the sleeve for $Re = 500, \bar{U} = -5.0$ and various $\bar{\epsilon}$.

An eddy, rotating counter-clockwise, is generated for an eccentricity as small as 0.2. From Fig. 3, the presence of the eddy does not restrict the flow through the slotted sleeve which is predominently through the side closest to the eddy. As the eccentricity is increased, the amount of fluid flowing through the contraction (the region where the sleeve is closest to the bowl) is reduced and more fluid now enters the annulus from the side closest to the eddy which is now moving in the direction of rotation of the bowl. This is verified from Table 1 which gives the eddy centre as well as the stream function (ψ_c) and vorticity (ζ_c) values there. According to Table 1, the vorticity at the eddy centre decreases, while the stream function at the eddy centre increases with increasing eccentricity.

$\bar{\epsilon}$	(x_c, y_c)	ψ_c	ζ_c
0.2	$(1.27, -0.87)$	0.75	1.20
0.5	$(2.25, -0.36)$	1.24	0.80
0.7	$(2.81, -0.21)$	1.43	0.67

Table 1: Values of ψ, and ζ at (x_c, y_c).

Fig. 3 shows the presence of stagnation points and suggests that the flow within the annular region is bidirectional. The same observation holds for the non-Newtonian case. Current study shows that upon increasing the speed of the rotor, the flow through the slotted sleeve and through the contraction become restricted causing the eddy centre to move in the direction of the rotation of the rotor. Also, for Reynolds number in the range $50 - 1000$ the flow fields obtained are qualitatively similar, although the computed values of the stream and vorticity functions are different.

Fig. 4 shows the vorticity along two diameters of the bowl that pass close to the slotted sleeve. The vorticity generated correspond to the problems $\{50.0, 0.5, -10.0\}$ and $\{1000.0, 0.5, -10.0\}$. The peaks indicate when the line is closest to the slotted sleeve. From these results, we can conclude that the vorticity generated along the no-slip surfaces is not diffused into the main flow domain. This is in contrast with the results obtained when the bounding cylinders rotate in the same direction (not shown here): the vorticity generated along the slotted sleeve is diffused into the main flow domain.

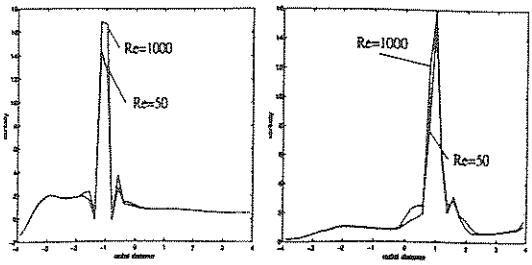

Figure 4: Vorticity along two lines.

2.2 Pseudoplastic Fluids

To study the flow of pseudoplastic fluids within the model, we fix the eccentricity ratio ($\bar{\epsilon}$), the fluid consistency coefficient (k_1) and the critical shear rate ($\dot{\gamma}_c$) at 0.7, 0.2 and 0.001, respectively. The flow fields presented here are used to study the effect of the dimensionless parameter S and the power law index α on the flow field. A more complete study is currently being done. In each of the diagrams given below, the contour lines and the apparent viscosity function are superimposed. The light regions denote regions of low shear or, equivalently, regions of high apparent viscosity. To study the effect of the parameter S, we solve the problems $\{0.2, 0.8, -5.0\}$, $\{1.0, 0.8, -5.0\}$ and $\{5.0, 0.8, -5.0\}$. This set notation defines, S, α and $\bar{U}$ respectively. The location and values of the stream function, vorticity function and apparent viscosity at the eddy center, together with the torque exerted along the rotor are given in Table 2. Fig. 5 shows the flow fields for the extreme values of S. From these figures we see that when $S = 5.0$ (the second figure), the apparent viscosity is diffused uniformly from the slotted sleeve into the main region; however, for the developed flow corresponding to the smaller value of S, the vis-

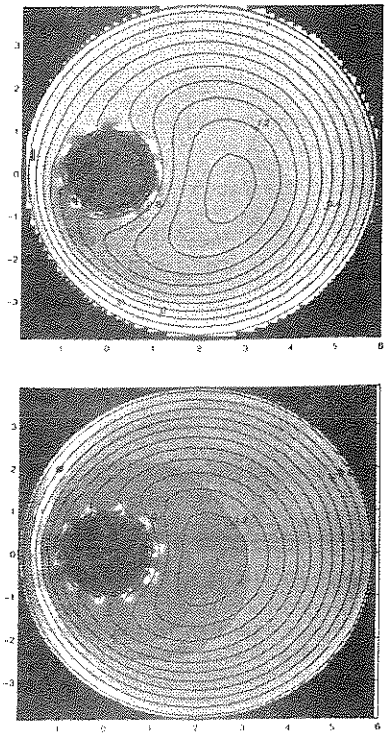

Figure 5: Contour plots in the flow field for $\alpha = 0.8, \bar{U} = -5.0$ and various S.

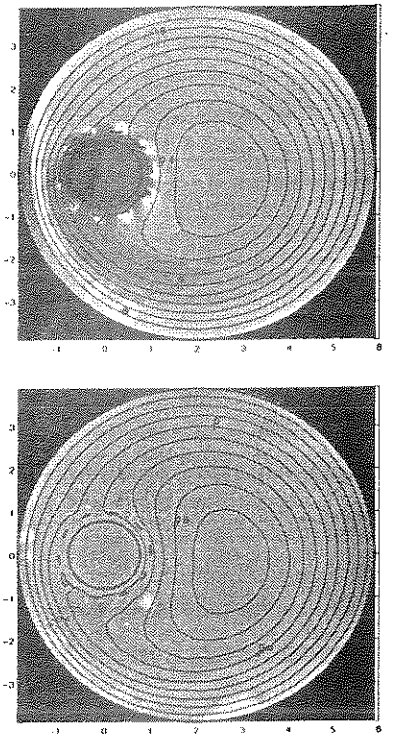

Figure 6: Contour plots in the flow field for $S = 0.2, \bar{U} = -2.0$ and various α.

S	(x_c, y_c)	ψ_c	ζ_c	h_c	T
0.2	$(2.81, -0.21)$	1.46	0.67	0.216	122.32
1.0	$(2.38, -0.31)$	1.43	0.67	0.216	132.21
5.0	$(2.38, -0.31)$	1.35	0.82	0.208	137.74

Table 2: Values of ψ, ζ and viscosity at (x_c, y_c) and torque along the rotor.

cosity is convected away from the sleeve by the fluid flowing through the contraction. This behaviour can be explained in two ways. From equation (1.1), S can be regarded as the diffusivity for both ζ and $h(\dot{\gamma})$. As S increases, the rate of diffusion of these functions is increased. The relationship between ζ and $h(\dot{\gamma})$ is seen in (1.8). The second explanation interprets the dimensionless parameter, S, as the ratio of shear forces to inertia forces. An increase in S corresponds to an increase in shear forces in the flow domain. As S is increased, the increase in shear forces is seen in Table 2 through the increase in the vorticity and the decrease in the apparent viscosity at the eddy center. From the contour plots, we see that increasing S produces a uniform diffusion of the apparent viscosity causing a more symmetric (about the horizontal) flow field and more fluid now flows through the contraction.

We now study the effect of varying the power law index, α. Upon increasing the non-Newtonian behaviour of the fluid, the torque around the rotor decreases and the apparent viscosity in the flow field is increased. Fig. 6 shows the flow fields corresponding to the problems $\{0.2, 0.8, -2.0\}$ and $\{0.2, 0.2, -2.0\}$. From these figures the change in the viscosity can be seen. For example, the low-shear regions behind each no-slip surface of the sleeve are removed as α is decreased, and the colour in the domain becomes more uniform indicating less variation in the apparent viscosity. From the contour lines, we see that as α is reduced, more fluid now flows through the region of the sleeve closest to the bowl than before and less fluid flows through the contraction; thus, causing the streamlines to become more circular.

3 CONCLUSIONS

The study outlined in this paper was undertaken to examine the behaviour of the fluid flow around a slotted sleeve placed concentrically around the interior cylinder of two eccentric rotating cylinders. The geometry used here represents a two-dimensional model of a viscometer designed to measure the rheological properties of settling slurries. There are many factors that affect the performance of this viscometer. Two important factors that can be easily studied are the amount of mixing present within the flow field and the location of low-shear regions. By determining the amount of mixing the fluid undergoes, the ability of the viscometer to maintain the homogeneity of the slurry can be assessed. Locating the regions of low shear rate may indicate where the particles in the slurry are concentrated. This phenomenon has been observed both experimentally and numerically by Than-Thien et al [1995] using particles suspended in a viscous Newtonian fluid placed between eccentric rotating cylinders (but without a slotted sleeve). From the results presented here, the mixing of the slurry is expected to be enhanced by moving the concentric system (i.e., the rotor and the slotted sleeve) closé to the rotating bowl and using low to moderate rotational speeds for the rotor and bowl. If the slurry is assumed pseudoplastic, then for slurries modelled using moderate to high values of the power law index, regions of low shear rate are located behind each surface element of the sleeve and close to the surface of the bowl. The apparent viscosity within the flow field is increased for slurries modelled using a large value for S, or for slurries possessing strong non-Newtonian behaviour (i.e., small α). An increase in the apparent viscosity can also be achieved by increasing the speed of the rotor but this will severely affect the mixing of the fluid.

References

Hird, L.D., and P.F. Siew. Small Reynolds number flow between eccentric rotating cylinders with a permeable sleeve. *J.Austral.Math.Soc.Ser.B*, 38(2):255–273, 1996.

Miller, J.J.H., and S. Wang. An exponentially fitted finite volume method for the numerical solution to 2d unsteady incompressible flow problems. *J.Comput.Phys.*, 115(1):56–64, 1994.

Overend, I.J., R.R. Horsley, R.L. Jones, and R.K. Vinycomb. A new method for the measurement of rheological properties of settling slurries, 1984.

Phan-Thien, N., A.L. Graham, S.A. Altobelli, J.R. Abbott, and L.A. Mondy. Hydrodynamic particle migration in a concentrated suspension undergoing flow between rotating eccentric cylinders. *Industrial Engineering and Chemical Research*, 34:3187–3194, 1995.

Sonneveld, P. CGS, a fast lanczos-type solver for nonsymmetric linear systems. *SIAM J.Sci.Stat.Comput.*, 10(1):36–52, 1989.

Tanner, R.I., and J.F. Milthorpe. Numerical simulation of the flow of fluids with yield stresses. In *Third International Conference on Numerical Methods in Laminar and Turbulent Flow.*, pages 680–690, Seattle, 1983.